



This is to certify that the

thesis entitled

QUANTITATIVE MORPHOLOGICAL CHARACTERIZATION OF TRIAXIALLY BRAIDED COMPOSITES USING IMAGE ANALYSIS

presented by

Li Jiang

has been accepted towards fulfillment of the requirements for

M.S. degree in Mechanical Engineering

Major professor

Date $\frac{7/28/9}{}$

MSU is an Affirmative Action/Equal Opportunity Institution

O-7639

LIBRARY Michigan State University

PLACE IN RETURN BOX to remove this checkout from your record. TO AVOID FINES return on or before date due.

DATE DUE	DATE DUE	DATE DUE
(te) > 715 162		

MSU is An Affirmative Action/Equal Opportunity Institution chirodelegus pm3-p.1

QUANTITATIVE MORPHOLOGICAL CHARACTERIZATION OF TRIAXIALLY BRAIDED COMPOSITES USING IMAGE ANALYSIS

By

Li Jiang

A THESIS

Submitted to
Michigan State University
in partial fulfillment of the requirements
for the degree of

MASTER OF SCIENCE

Department of Mechanical Engineering

ABSTRACT

QUANTITATIVE MORPHOLOGICAL CHARACTERIZATION OF TRIAXIALLY BRAIDED COMPOSITES USING IMAGE ANALYSIS

By

Li Jiang

The prediction of mechanical properties of reinforced composites is strongly influenced by the morphological features of the reinforcement. In order to improve the correlation between predicted properties and test properties, it is essential to have quantitative measures of the composite morphologies. Methods were developed to quantify braid angle, crimp angle and fiber waviness using computer-aided image processing techniques. The braid angle and fiber waviness at a sample surface are determined non-destructively. Cutting is presently required to determine the crimp angle. The determination of braid angle is based on the fast Fourier transform (FFT) method, while the crimp angle determination is accomplished using edge detection and boundary identification. Strategies have been proposed to quantify fiber waviness. Calibration tests were conducted to compare computer-based pattern recognition with human determinations. The reproducibility of the measurements is quantified. Extensions of this study have the potential to provide automated, on-line quantitative measurements of composite geometrical features which are important for quality control and engineering design.

ACKNOWLEDGMENTS

I would like to thank my major professor Dr. John J. MaGrath for his guidance and support throughout this work.

Thanks are given to Dr. Anil Jain, graduate students Chitra Dorai and Patchrawat Uthaisombut, Department of Computer Science for their help with the image acquisition. Also I would like to thank Dr. Dennis Gilliand, graduate student Hao Zhang, Department of Statistics and Probability and Dr. Alan Haddow, Department of Mechanical Engineering for their helpful discussions and suggestions concerning this work.

I am grateful for the financial support of this project from the Research Excellence Fund of the State of Michigan.

Finally, I would like to express my deep appreciation to my family, my husband and my parents for their love and encouragement.

TABLE OF CONTENTS

LI	LIST OF TABLES vi		
LI	ST C	PF FIGURES	
1	INI	RODUCTION	
	1.1	Motivation 1	
	1.2	Literature Review	
2	IMA	AGE PROCESSING	
	2.1	Introduction	
	2.2	Image Enhancement	
		2.2.1 Histogram Equalization	
		2.2.2 Lowpass Filtering	
		2.2.3 Edge Detection	
	2.3	Thresholding	
	2.4	Morphological Filters	
	2.5	Thinning	
	2.6	Fast Fourier Transform	
3	QU.	ANTIFICATION OF MORPHOLOGICAL FEATURES	
	3.1	Introduction	
	3.2	Image Analysis System Setup	
	3.3	Errors in Measurements	
	3.4	Braid Angle Determination	
		3.4.1 Calibration	
		3.4.2 Sample Image Analysis	
	3.5	Crimp Angle Determination	
		3.5.1 Calibration	
		3.5.2 Sample Image Analysis	
	3.6	Fiber Waviness Determination	
4	RES	SULTS AND DISCUSSIONS	
	4.1	Braid Angle Determination	

		4.1.1 Calibration	62
		4.1.2 Sample Image Analysis	67
	4.2	Crimp Angle Determination	
		4.2.1 Calibration	69
		4.2.2 Sample Image Analysis	70
	4.3	Image Analysis Speed	
5		NCLUSIONS AND RECOMMENDATIONS	
	5.1	Conclusions	79
	5.2	Recommendations for Future Work	81

LIST OF TABLES

Table 1	Calculated Results of Ten Measurements of Each True Angle (Unit: deg)
Table 2	Calculated Results from Least-Squares Curve Fit 65
Table 3	Comparison of the Least-Squares Method with the Manual Measurement for Test Images (Unit: deg) 65
Table 4	Braid angles at Different Locations (Unit: deg)
Table 5	Comparison of Braid Angle Measurements between the Least-Squares Method and the Manual Measurement (Unit: deg)
Table 6	Crimp Angles from Test Images (Unit: deg)
Table 7	Crimp Angles from Nine Specimens (Unit: deg)
Table 8	Reproducibility of the Crimp Angle Measurement Tested by Repeating Imaging on One Specimen (Unit: deg)
Table 9	Reproducibility of the Crimp Angle Measurement Tested by Repetitions of Measurement on One Image (N=5) (Unit: deg) 77

LIST OF FIGURES

Figure 1	Definition of braid angle 5
Figure 2	Definition of crimp angle 7
Figure 3	Definition of fiber waviness
Figure 4	Original image
Figure 5	Image in Figure 4 after histogram equalization
Figure 6	Schematic of digital convolution
Figure 7	Image produced by applying a 3 x 3 lowpass filter 16
Figure 8	A 3 x 3 Laplacian kernel
Figure 9	Result of applying a 3 x 3 Laplacian
Figure 10	Schematic of Sobel filtering
Figure 11	Sobel kernels
Figure 12	Image produced by applying Sobel filter
Figure 13	Effect of applying Phase filter
Figure 14	Image in Figure 7 after thresholding
Figure 15	Original test image
Figure 16	Two repetitions of a 5 x 5 Dilation
Figure 17	Two repetitions of a 5 x 5 Erosion
Figure 18	Original test image

Figure 19	Image obtained by applying Opening
Figure 20	Image obtained by applying Closing
Figure 21	Example test image
Figure 22	FFT image
Figure 23	Schematic of the image analysis system
Figure 24	(a) Example test image for calibration of braid angle analysis (b) The fast Fourier transform of (a)
Figure 25	Test FFT image for calibration of braid angle analysis 43
Figure 26	Final thinned image
Figure 27	 (a) The whole part (~1.5 m long) (b) A closer picture of the part surface (c) The cross section of the part (80 x 32 mm²) The bright section is the foam core
Figure 28	Example image from the sample surface after histogram equalization
Figure 29	The FFT of image in Figure 28
Figure 30	Image produced by applying Dilation and Erosion operations 49
Figure 31	Image in Figure 30 after Laplacian edge detection 49
Figure 32	Inverse transformation of the modified FFT in Figure 29 51
Figure 33	Polynomial test image for calibration of crimp angle analysis 53
Figure 34	Image after thresholding 53
Figure 35	Image in Figure 34 after thinning
Figure 36	Example raw crimp image for crimp angle determination 56
Figure 37	Image in Figure 36 after histogram equalization 56
Figure 38	Image in Figure 37 after applying a lowpass filter
Figure 39	Image in Figure 38 after applying a Laplacian edge filter 57

Figure 40	Image in Figure 39 after thresholding
Figure 41	Image in Figure 40 after applying Sobel filter
Figure 42	Image in Figure 40 after thinning
Figure 43	Example raw image of fiber waviness after histogram equalization
Figure 44	Image in Figure 43 after applying a vertical edge filter 60
Figure 45	Image in Figure 44 after applying Phase filter and thresholding
Figure 46	Image in Figure 45 after thinning
Figure 47	Example of least-squares line fit to data points
Figure 48	Example of 7th order polynomial function fit to the fiber boundary
Figure 49	Crimp angles measured on different specimens
Figure 50	Crimp angle distribution over one sample

CHAPTER 1

INTRODUCTION

1.1 Motivation

In the development of new materials, fiber-reinforced composites have occupied an extremely important role. Compared with traditional materials, these composite materials offer some significant advantages, such as larger strength-to-weight ratios, as well as increased stiffness and tensile strength in the direction of fiber orientation. Such composites are more flexible in bending and the thermal stability is improved because of their lower coefficients of thermal expansion. Therefore, fiber-reinforced composites have been widely used in many applications. Specifically, they have been found to be extremely suitable for the automotive and aerospace industry.

Fiber-reinforced composites consist of fibers and the surrounding matrix.

The reinforcing fibers can be in continuous lengths or in discontinuous lengths. In general fibers are the major load-carrying components, while the roles of the matrix are to transfer stresses between the fibers, provide an

environment to make the fibers in the desired location and protect the fibers from environmental damages.

One advantage provided by fiber-reinforced composites is the ability to be tailored to meet different requirements. In automotive applications, when applying composites to structural components, "engineered" architectures are required. Specific needs can be satisfied by varying the glass fiber orientations and volume fractions.

The morphologies of the reinforcement strongly influence the material properties of fiber-reinforced composites, although their roles have not been completely understood. In order to predict material properties it is important to understand the relationship between manufacturing parameters and geometrical structures.

It has been found that braiding of glass fiber offers potential cost effectiveness. It is good for tubular structures and allows tailoring of preform architecture to adjust strength and stiffness. Investigations of elastic properties of
triaxially braided glass/urethane composites have been performed by Ford
research engineers. Process science models which relate the yarn size, braid
angle, number of yarns and mandrel diameter to the fiber volume fraction and
internal geometry etc. have been developed (Jaranson et al., 1993).

It was found that during the sample manufacturing process, some problems were encountered. First, braid angles which were less than 35° were loose and difficult to handle. Therefore the final braid architecture was distorted. Second, all the braids tended to be unstable after they were cut from the mandrel. This resulted in ±10° braid angle variations. Third, at the point of injection, additional distortion occurred and the braid architecture got worse (Jaranson et al., 1993). A comparison of the elastic properties between experimental results and theoretical results has been made. The correlation between experimental and theoretical results was not satisfied.

In order to improve the correlation between predicted properties and test properties, it is essential to have accurate quantitative measures of morphologies of composites. The objective of this study is to develop methods quantifying the morphological features of the triaxially braided composites using computer-aided image processing techniques. These morphological features include braid angle, crimp angle and fiber waviness. The final application of the techniques being developed could be applied to the production line to provide a means of engineering design and quality control. Therefore the methods desired should be non-destructive, accurate, automated, rapid, and economical. The long term goal of this study is to automate the whole process as much as possible. Although it seems impossible to give an accurate absolute description of the composite morphology, it has been shown that computer-based determinations are at least as accurate as human-based determinations and can give results with an acceptable accuracy for a specific application.

1.2 Literature Review

Masters et al. (1993) studied the role of the braid reinforcement microgeometry in laminate mechanical behavior. The unnotched tensile properties and fiber volume fractions were investigated for two-dimensional triaxial braid-reinforced graphite/epoxy composites both experimentally and analytically. The material sensitivity was tested by varying the braid angle, the yarn sizes and the longitudinal yarn content. A process science model which relates the braid architectures to machine parameters was developed.

The definition of the braid angle which is shown in Figure 1 is the absolute angle between the longitudinal tow (0° direction tow) direction and the braid tow direction. Trace yarns were formed by coating graphite yarns with nickel to determine the locations of yarns. Scanned surface images were produced. Braid angles were measured using image analysis software by tracing the nickel-coated yarns. Longitudinal cross sectioning, transverse cross sectioning and cross sectioning along the braid yarns were conducted to exam the internal fiber architecture.

Jortner (1989) investigated a carbon/carbon laminate reinforced with plain-woven cloth. He found that tensile strength variations were quite related to variations in the crimp angle of the interwoven yarns. Small crimp angles were associated with high strengths. He also found that the ultimate load per yarn was proportional to the inverse of the sine of the average maximum crimp angle. Crimp angles were measured manually with the aid of a protractor scale which was attached to the microscope's ocular.

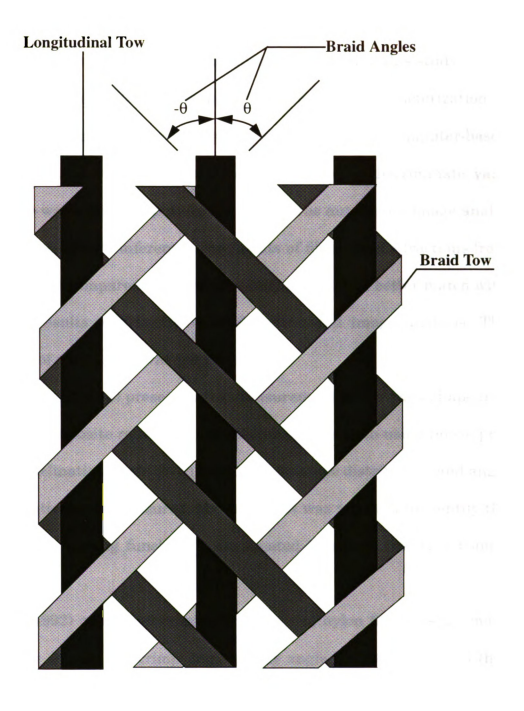


Figure 1. Definition of braid angle.

The crimp angle can be defined in different ways. One commonly used definition defines the crimp angle over one fiber yarn peak and trough as the maximum absolute angle between the mean yarn direction and the tangent line of the yarn as shown in Figure 2. This definition is also used in this study.

Gowayed and Russ (1991) presented the geometrical characterization of triaxially braided carbon/epoxy composite preforms using computer-based analysis techniques. Two approaches were conducted to discriminate yarn locations. One was manual input, the other one was automated image analysis with minimal human inference. The results of fiber volume fractions from each method were compared with the experimental data. A better match with experimental results was found by using automated image analysis. The quantification of yarn shape was not reported.

Yurgartis et al. (1993) presented the measurement of the yarn shape in a carbon/carbon composite reinforced with a plain weave cloth using image processing. The inclination angle distribution, crimp angle distribution and angle match distribution were measured. Manual input was required to identify the yarn boundaries. Fitting functions were created to match the yarn boundaries.

Xu et al. (1992) quantified crimp morphology of nylon fibers using image analysis. They defined the crimp angle as the angle between two lines that were tangent to two shoulders of a crimp at the points of maximum slope. Processing operations were created to transform the original digitized image in order to enhance the fiber boundary. The images they used contained only

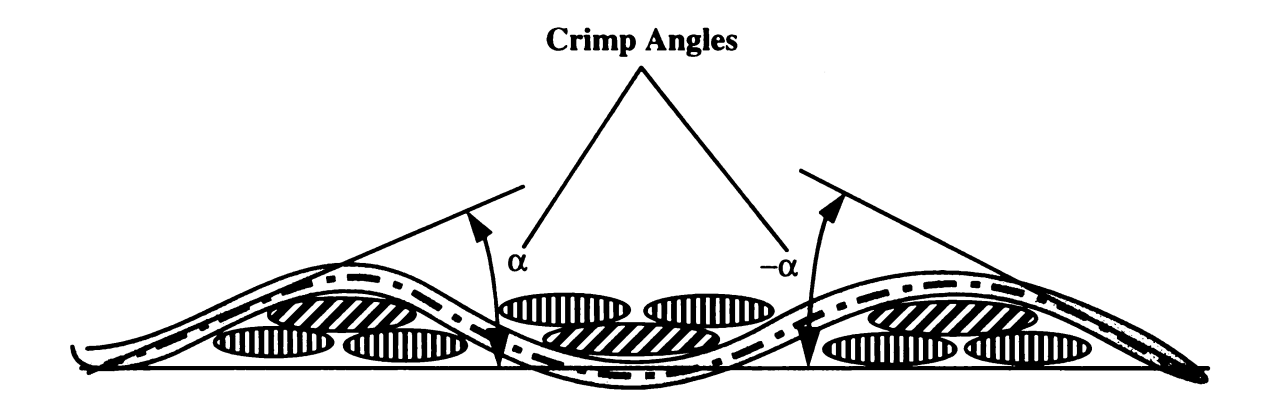


Figure 2. Definition of crimp angle.

fibers without the presence of any complexity introduced by the background.

Yurgartis (1987) suggested that the fiber misalignment in continuous fiber composite had been suspected of having a significant influence on composite properties such as longitudinal compression strength and longitudinal tensile modulus etc.. A method to measure small angle fiber misalignments (fiber waviness) in continuous non-woven fiber composites was developed. Fiber misalignment distributions were determined. Characterization of the fiber curvature was not given.

Rai et al. (1992) studied the relationship between lamina stiffness and fiber waviness of carbon-epoxy composites. A unidirectional lamina elastic model was developed where the fiber was assumed to be sinusoidal. It was found that the stress-strain response to non-zero fiber waviness was nonlinear. It was concluded that having quality control of fiber waviness in structural applications was a very critical issue. In their study the fiber shape is represented by a sinusoidal function which is shown in Figure 3:

$$y = A \sin\left(2\pi \frac{x}{L}\right) \tag{1}$$

where A is the amplitude and L is the wave length of the sinusoidal function. The ratio of A to L is defined as fiber waviness which can be calculated from the measured maximum absolute fiber angles.

Many efforts have been made by numbers of researchers to study the effects of geometrical features of reinforcing fibers on composite properties.

Although the influences can not be completely explained, the conclusion of the importance of these geometrical features is clear. Accurate and effective methods for quantitatively characterizing composite morphologies are needed.

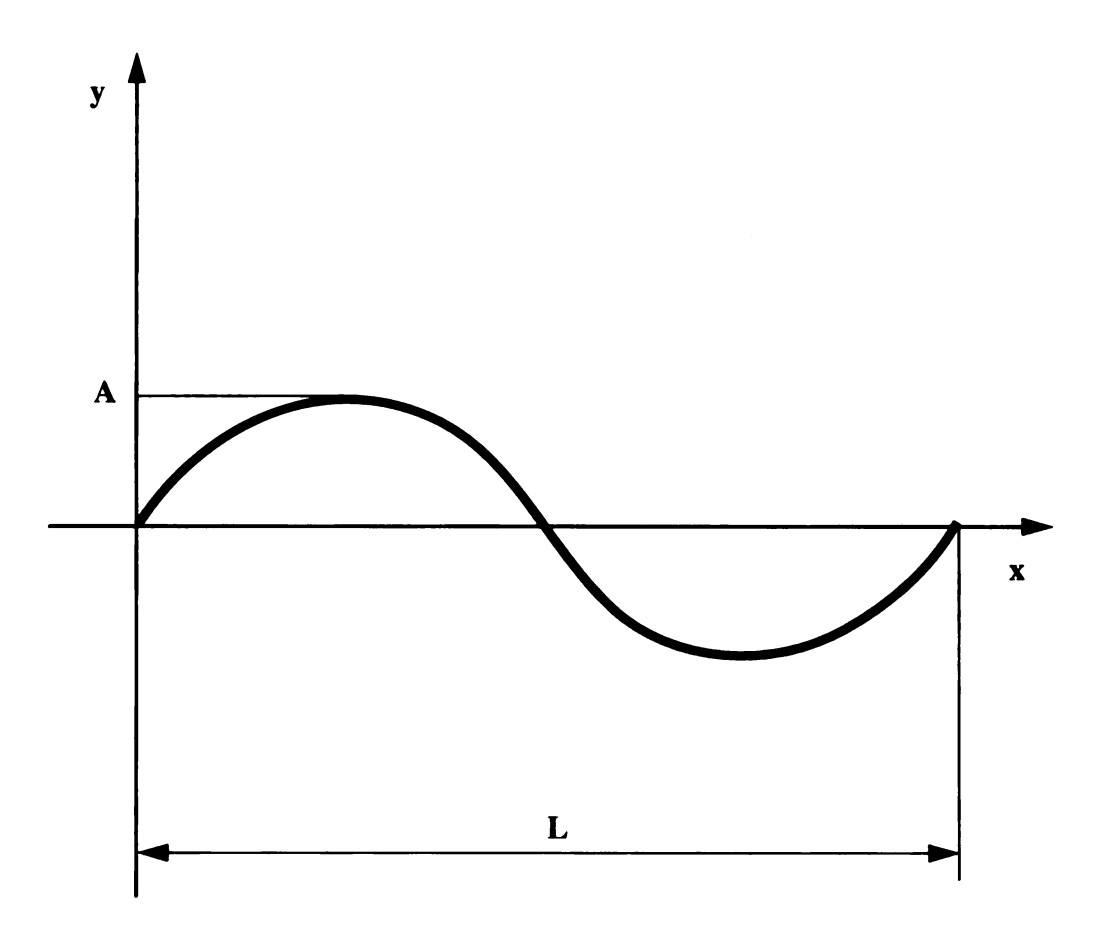


Figure 3. Definition of fiber waviness.

CHAPTER 2

IMAGE PROCESSING

2.1 Introduction

Computer-based imaging analysis provides a powerful tool for the characterization of composite materials. Recognizing and measuring features and structures can be performed very quickly with good reproducibility. Recently image processing techniques have become increasingly important in the study of composite materials.

Since computers can only process numerical data an image must be converted to numerical form before computer processing. This conversion process is called digitization. After an image is captured in digital form it is then sampled into a set of points which can be represented by a matrix. Each point is called a picture element or a pixel. An integer value called the grey level is generated at each pixel. This process is called gray-level quantization. For 8-bit data acquisition as performed here, index values between 0 and 255 (28 = 256 grey levels) are used to represent all gray levels between black and

white.

In order to get a desired output image, image processing operations are applied to the digitized image. These operations involve image enhancement, image segmentation, morphological operations etc. The effect of each operation can only be described in general. One can not predict the exact result a particular filter will have on a particular image. The computer does not always give the results that a person may expect. The operator has the ultimate authority to judge the quality of an image to decide if a processed image is good enough for a specific application. One must go through a trial-and-error process which means that different types of filters should be tried until the satisfied results are obtained.

In this study a commercial imaging processing program (Image-Pro Plus) is used to perform image transformations. The image processing operations which were applied in this study will be described in the following sections.

2.2 Image Enhancement

2.2.1 Histogram Equalization

The gray level histogram is used to represent the grey level distribution in an image. It shows whether an image is too bright or too dark. An image is well scaled when it makes use of all the available gray levels. When the histogram fills the entire gray value range from 0-255, the grey level distribution is

optimal. For a given image, some gray values may not be used due to the poor contrast of the object or the image acquisition process. This can be improved using histogram equalization. Histogram equalization alters the contrast of an image and makes the distribution of grey level uniform by assigning new intensity values to the original image pixels. The order of the brightness of each pixel remains unchanged. Only the values change to the new ones. This forces the peak areas in the histogram to spread out and the trough areas to compress. The transformation process can be expressed as:

$$S_{j} = \sum_{i=0}^{j} \frac{N_{i}}{N}$$
 $j = 0, 1, 2, \dots, k-1$ (2)

where k is the number of grey levels, S_j is the new assigned value for the jth gray level, N_i is the number of pixels having ith gray level, and N is the total number of pixels. After equalization, the original gray values are mapped to the new values. The modified image remarkably improves the dynamic range of the image as well as the visibility of features of interest. Example images are given below. Figure 4 shows an original image. The image in Figure 4 after histogram equalization is illustrated in Figure 5.

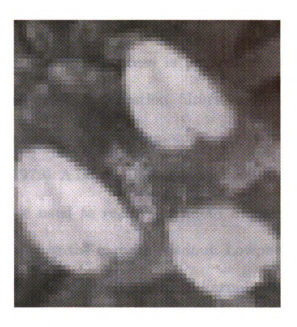


Figure 4. Original image.



Figure 5. Image in Figure 4 after histogram equalization.

2.2.2 Lowpass Filtering

Based on how the filtering process is performed, spatial filters can be divided into two categories: convolution filters and nonconvolution filters. Convolution is commonly used to implement linear operations on signals and images (Castleman, 1979). A lowpass filter is a convolution filter.

Lowpass filters are used to remove random image noise which may be caused from the lighting or the camera readout. Lowpass filtering operations are accomplished by kernel multiplications. A kernel multiplication is the convolution of a filter kernel with the original image. The whole process can be described as follows: each pixel of the filter kernel is multiplied by the corresponding pixel of the image kernel, add the results, then divide the sum by the sum of the filter kernel. Figure 6 shows the schematic of digital convolution. Applying a 3 x 3 lowpass filter to the original image in Figure 4 yields the image in Figure 7.

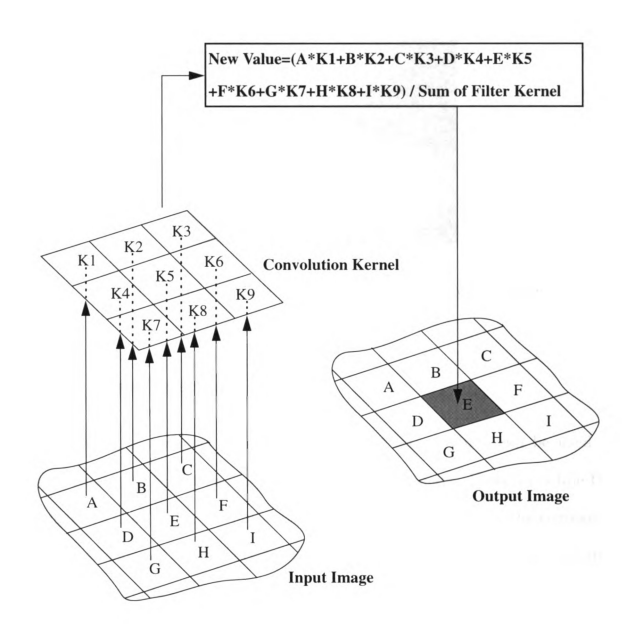


Figure 6. Schematic of digital convolution.

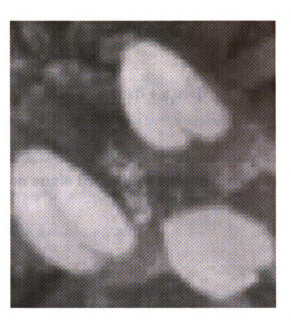


Figure 7. Image produced by applying a 3 x 3 lowpass filter.

2.2.3 Edge Detection

There are a variety of edge enhancement filters which can be used to accentuate the high frequency information in an image. However, while the edges are sharpened, the noise may also be enhanced. One of the commonly used techniques for edge enhancement is differentiation. For a given function f(x, y), the gradient of f is defined as:

$$g[f(x,y)] = \begin{pmatrix} \frac{\partial f}{\partial x} \\ \frac{\partial f}{\partial y} \end{pmatrix} = \begin{pmatrix} g_x \\ g_y \end{pmatrix}$$
 (3)

For any vector direction l, the directional derivative is:

$$\frac{\partial f}{\partial l} = g_x \cos \beta + g_y \sin \beta \tag{4}$$

where β is the rotation angle from the x axis to direction l. The magnitude of g[f(x, y)] is:

$$Mag(g) = \sqrt{g_x^2 + g_y^2}$$
 (5)

For a digital image, the derivatives in the equations above can be approximated using difference approximations. Many approximation methods may be used, such as forward difference approximation which can be expressed as:

$$\frac{\partial f}{\partial x} = f(x+1, y) - f(x, y)$$

$$\frac{\partial f}{\partial y} = f(x, y+1) - f(x, y)$$
(6)

The second derivatives are defined as:

$$g_{xx} = \frac{\partial^2 f}{\partial x^2}$$

$$g_{yy} = \frac{\partial^2 f}{\partial y^2}$$
(7)

The reason for using the gradient for edge enhancement is that the direction of the gradient indicates the direction of the maximum rate of increase of the function f(x, y), and the magnitude of the gradient is the maximum rate of increase of f(x, y) per unit distance in the direction of the gradient (Gonzalez and Wintz, 1977). In an image, the gradient values will be larger in regions having rapid variations and smaller in smooth regions.

The Laplacian which is defined as:

$$L = \frac{\partial^2 g}{\partial x^2} + \frac{\partial^2 g}{\partial y^2} \tag{8}$$

is a second derivative convolution operator. The second derivative will also identify the maximum gradient because the second derivative changes sign at a position where the first derivative is a maximum. A typical 3 x 3 Laplacian kernel is shown in Figure 8.

0	-1	0
-1	4	-1
0	-1	0

Figure 8. A 3 x 3 Laplacian kernel.

As we can see, the kernel has zero weighting (the sum of the kernel elements is zero). This indicates that the result of applying a Laplacian kernel to a constant brightness image region will be zero. Also because of the central weighting in the kernel, the Laplacian will respond strongly to points, lines and edges. It is direction-invariant. The result of applying a 3 x 3 Laplacian operator to the image in Figure 4 is shown in Figure 9.



Figure 9. Result of applying a 3 x 3 Laplacian.

The Sobel filter is a nonlinear edge detector and it is strongly directional. Figure 10 illustrates the process of Sobel filtering. Typical 3 x 3 Sobel kernels are shown in Figure 11. Figure 12 illustrates the image produced by applying the Sobel filter to the original image.

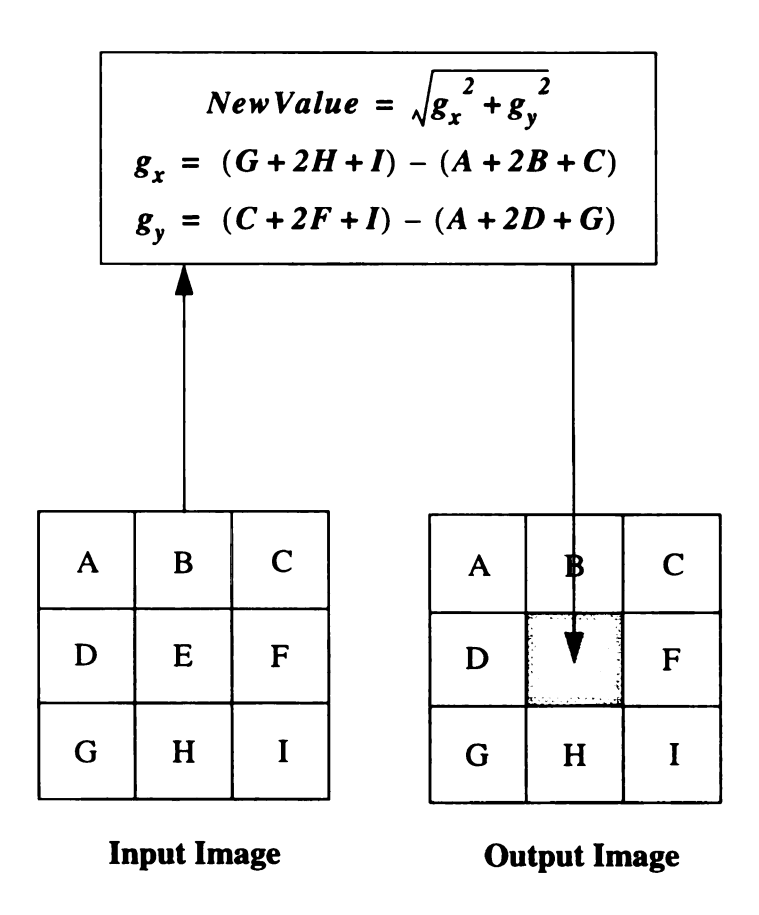


Figure 10. Schematic of Sobel filtering.

1	2	1
0	0	0
-1	-2	-1

1	0	-1
2	0	-2
1	0	-1

Figure 11. Sobel kernels.

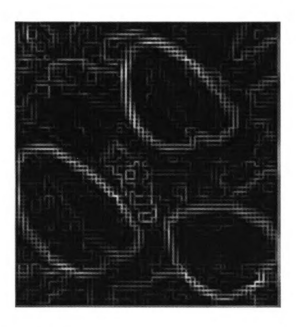


Figure 12. Image produced by applying Sobel filter.

Another edge detection filter called Phase which measures the direction of the gradient:

$$Direction = arctan \left(\frac{g_y}{g_x} \right)$$
 (9)

Phase filtering is the complement of Sobel filtering. For each pixel, the gradient direction is assigned a value. Then this value is scaled to the gray scale such that each direction can be represent by a corresponding gray value. The example image given in Figure 13 is obtained by applying the Phase filter to the image in Figure 7 after thresholding.



Figure 13. Effect of applying Phase filter.

2.3 Thresholding

After an image is captured and digitized, different image enhancement operations may be performed in order to get a desired image. The purpose of doing these operations includes correction of defects in the original image, removal of noise, increasing the visibility of features of interest and extracting the useful information. Such improvement will make the image suitable for further analysis and measurements. Before conducting measurements, image segmentation should be performed. Segmentation is a process that attempts to separate touching features in an image. Thresholding is one of the image segmentation methods. By thresholding, a gray scale image is converted to a binary (black and white) image where the features of interest in the image are discriminated from the others. Either the features of interest or the background can be assigned as black or white. In this study, fibers are set to white, the matrix is set to black.

Manual setting of threshold values is commonly used. The operator is responsible for defining the threshold values by inspection of the image. Changing threshold values (from 0 to 255), the operator observes each corresponding binary image, a threshold is set when the operator makes the decision that the regions of interest are well separated from the background. Unlike other edge detection operations, thresholding processes the entire image at once. So it is time saving and more efficient. On the other hand, thresholding may introduce errors to the measurement results. The critical issue associated with the thresholding operation is to set a proper threshold in

order to keep the size of the binary object as close as possible to the one in the original gray scale image. However it is impossible to get an exact match. Errors introduced by thresholding and the way to reduce them will be discussed in section 3.5.2. An example image obtained by thresholding the image in Figure 7 is shown in Figure 14.



Figure 14. Image in Figure 7 after thresholding.

2.4 Morphological Filters

Morphological processing provides a different way to modify both gray scale images and binary images. There are two basic morphology operators: Dilation and Erosion (Russ, 1990). In a binary image there are only two possible values (1 or 0) for each pixel. Dilation processing can be described as follows. A binary pixel having value 0 will be changed to 1 if any of its neighbors are 1. This results in adding one layer of pixels around boundaries of objects. Therefore Dilation will expand the object size and connect discontinuous regions. Erosion is a complementary operation relative to Dilation. If a pixel is 1, then it will be set to 0 if any of its neighbors are 0. Therefore one layer of pixels will be removed from around boundaries of objects. As a result of Erosion, the object will be reduced in size, and some continuous features may be broken. Figure 15 shows an example test image. The result of performing two repetitions of a 5 x 5 Dilation to the original image is illustrated in Figure 16. Two repetitions of a 5 x 5 Erosion on the original image produce the image in Figure 17.

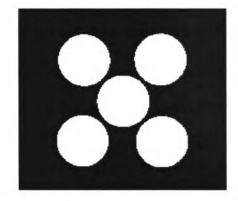


Figure 15. Original test image.

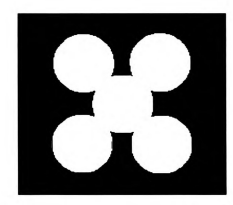


Figure 16. Two repetitions of a 5 x 5 Dilation.



Figure 17. Two repetitions of a 5 x 5 Erosion.

The Opening operation is formed by performing an Erosion followed by a Dilation respectively. It separates connected objects or opens the large enclosed holes near object borders. Since Erosion reduces the original object size while the following Dilation adds more pixels to the eroded object, the object dimension will be restored somewhat. However the overall size of the object will tend to be slightly smaller than the original one.

The Closing operation is formed by performing a Dilation followed by an Erosion respectively. Thus, Closing fills small holes and joins gaps in the object. The difference between the processed and original object size is smaller compared with using Opening. Since both Opening and Closing tend to remove small features from the object, the final image will look smooth and clean.

The applications of Dilation and Erosion may introduce distortion of the object shape. It is recommended to use the same kernel shape and the same number of cycles for both Dilation and Erosion for the purpose of reducing image distortion. An example test image is shown in Figure 18. The result of applying a 5 x 5 Opening is shown in Figure 19. Figure 20 illustrates the image obtained by applying a 5 x 5 Closing to the original image.

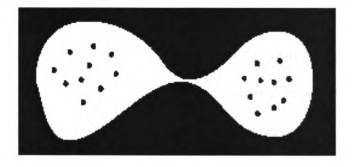


Figure 18. Original test image.

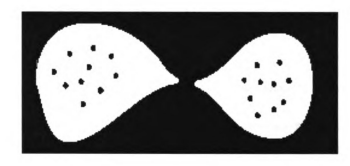


Figure 19. Image obtained by applying Opening.

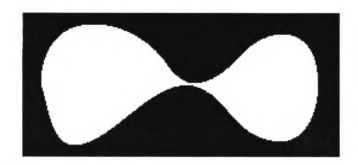


Figure 20. Image obtained by applying Closing.

2.5 Thinning

Thinning removes the exterior border pixels layer by layer until the object has a single pixel width. The connectivity of the image should be maintained after thinning. There are different thinning techniques. One method is to compute the shortest distance between each point in the object and a boundary point (Hussain, 1991). If more than one boundary points have the same minimum distance, then the corresponding object point is called a medial axis transformation point. During processing, all the pixels are removed except those which are medial axis transformation points. The final thinned object is called the medial axis of the object.

Thinning is very sensitive to changes of the object shape. Even a little change may produce some additional branches, loops or other complicated features. This will make the quantitative analysis difficult and the results may be unreliable. If the thinned image is too complicated, it will be impossible to interpret it. Therefore it is very important to produce an image with nice shaped objects before performing thinning.

2.6 Fast Fourier Transform

The image processing operations described in the previous sections are performed in the spatial domain, while the Fourier transform is a frequency domain operation. It plays an important role in the image processing analysis. Specifically, it has been found to be quite a useful tool for non-destructive evaluation (Blake, 1987). In the frequency domain, an image is represented by the energy spectrum represented as "white spots" which are symmetric about the origin. For each point, the brightness is proportional to the amplitude of the waveform. The direction from the origin indicates the direction of the waveforms.

For a two-dimensional continuous function f(x, y), the Fourier transform is defined as:

$$F(u,v) = \int_{-\infty}^{\infty} \int_{-\infty}^{\infty} f(x,y) e^{-j2\pi (ux+vy)} dxdy$$
 (10)

And, the inverse Fourier transform of F(u, v) is:

$$f(x,y) = \int_{-\infty}^{\infty} \int_{-\infty}^{\infty} F(u,v) e^{j2\pi(ux+vy)} dudv$$
 (11)

where u and v are frequency variables which correspond to the x and y directions.

For the discrete case, the image is divided into a $M \times N$ grid with a dimension of $\Delta x \times \Delta y$ for each unit cell. The two-dimensional discrete Fourier transform is given as:

$$F(u, v) = \frac{1}{MN} \sum_{x=0}^{M-1} \sum_{y=0}^{N-1} f(x, y) e^{-j2\pi \left(\frac{ux}{M} + \frac{vy}{N}\right)}$$

$$u = 0, 1, 2, \dots, M-1 \qquad v = 0, 1, 2, \dots, N-1$$
(12)

and the inverse transform of F(u,v) is:

$$f(x,y) = \sum_{u=0}^{M-1} \sum_{v=0}^{N-1} F(u,v) e^{j2\pi \left(\frac{ux}{M} + \frac{uy}{N}\right)}$$

$$x = 0, 1, 2, \dots, M-1 \qquad y = 0, 1, 2, \dots, N-1$$
(13)

Here, f(x, y) represents an image and F(u, v) is its spectrum. From the separability property of the two-dimensional Fourier transform, F(u, v) and f(x, y) can be obtained by applying one-dimensional Fourier transforms and the corresponding inverse transforms.

The fast Fourier transform algorithm is a decomposition procedure which reduces the numbers of multiply and add operations involved in the above equations. Especially when M and N are large, a great amount of time can be saved for the computation. More details about the Fourier transform and the fast Fourier transform can be found in Gonzalez and Wintz (1977). Figure 21 and Figure 22 show an example test image and its FFT respectively.

In the spatial domain, a convolution operation is performed by kernel multiplication. While in the frequency domain, the spectrum may also be modified using filters. A convolution operation can be achieved by multiplying the



Figure 21. Example test image.



Figure 22. FFT image.

transformed image by the kernel. Applying different filters allows low frequencies or high frequencies to be enhanced to smooth or sharpen the image and remove the other frequencies.

In the FFT, a certain pattern may be recognized from the spectrum direction. For example, if the fibers are aligned horizontally, then in the FFT the spectrum will distribute vertically and vice versa. This suggests the possibility of using FFT for the braid angle determination in this study and it has been proved to work well. Frequencies correspond to the noise and undesired background with known patterns in the FFT image can be easily cut off. After filtering operations, the image can be restored using the inverse transform.

CHAPTER 3

QUANTIFICATION OF MORPHOLOGICAL FEATURES

3.1 Introduction

The image processing method provides a means of performing pattern recognition and measurement. It has been proved to be an especially useful tool to conduct the morphological analysis and quantification of composite materials with good reproducibility.

The object of this study is to develop methods for quantifying morphological features of triaxially braided glass/urethane composites using computer-aided image processing techniques and automate the whole process as much as possible. The approach to braid angle determination used here is non-destructive and is based on the Fast Fourier transform method, while the approach to crimp angle determination involves edge detection and boundary identification. Cutting samples is required presently for the latter.

It should be noted that the quality of the image is very important in the

application of image analysis. It will directly affect the reliability of measurement results. A good quality image can minimize or eliminate problems later in the image processing. One can not totally rely on image operations. In other words, if problems associated with an image can be solved by the choice of cameras, optics or lighting systems, one should solve those problems directly and not by applying image operations.

3.2 Image Analysis System Setup

Image analysis procedures start with the image acquisition. The image is captured by a video camera which converts an optical image into an electrical signal. This analog signal is sent to the analog-to-digital converter (frame grabber) where the analog signal is converted into numerical data in the form of an array of numbers. Then these numbers are stored in the computer memory and they are ready for image processing.

Figure 23 shows the schematic of the image analysis system. Some of the images used in this study were captured in our lab using a Javelin Mos Sensor camera and a Sony DXC-151A CCD video camera. A Canon 16-100 mm TV Zoom lens and a Navitar Zoom 6000 lens were used to get different magnifications. Some of the images were captured in Dr. Anil Jain's lab in the Department of Computer Science, Michigan State University using a Panasonic GP-KR202 CCD video camera. The image digitization is done with a DT2861 image board which has a resolution of 512 x 480 pixels and provides 256 gray

levels. Image processing is performed using commercial software (Image-Pro Plus Version 2.0 and Version 1.2 for Windows) installed in a Gateway 2000 4DX2-66E PC. Images are displayed on a Electrohome No. 38-D05IMA-UP RGB monitor. A Conner backup hard disk tape drive is used to archive images. A 200MB magnetic tape can store about 800 images (512 x 480 pixels). It takes approximately one minute and forty seconds to store a 0.25MB image.

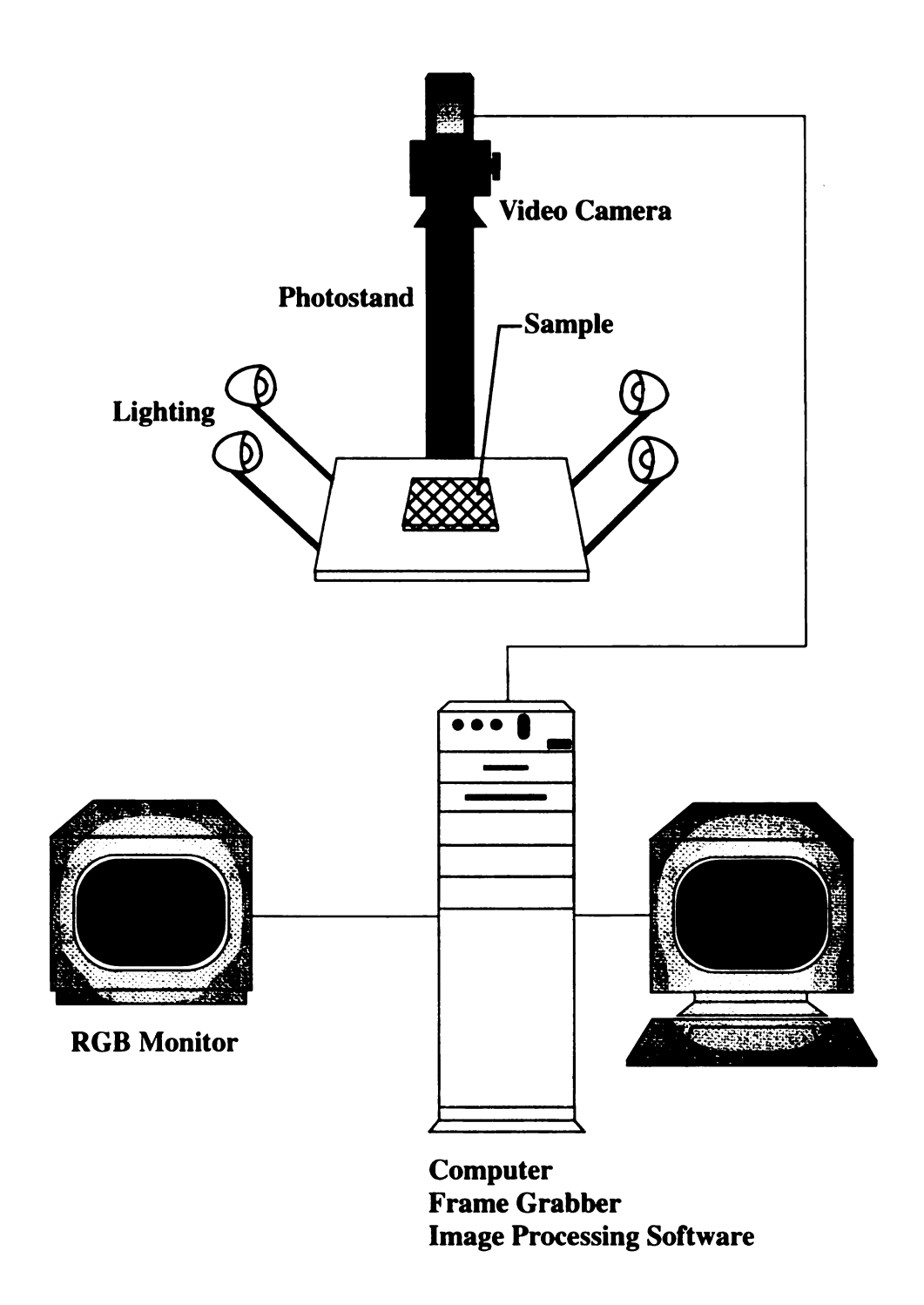


Figure 23. Schematic of the image analysis system.

3.3 Errors in Measurements

No measurement can be completely free of uncertainties. When a measurement is made, it is desired to know if the result is good enough. To be able to evaluate the uncertainties and keep them to a minimum is very important for any measurement.

"Error" by definition is the inevitable uncertainty that attends all measurements. It can not be avoided by being careful (Taylor, 1982). Errors can be grouped as random and systematic. Random errors can be estimated using statistical methods, while systematic errors can be hard to detect or evaluate, and can not be discovered by repeating measurements or increasing the sample sizes. They tend to accumulate and bias the measurement results. However if they are identified they can be corrected or reduced to magnitudes as small as possible. For a large reduction of both random errors and systematic errors, it is required to improve the techniques and the equipment used in the measurement.

For any experimental result, it is also desired to have a quantitative estimation of the measured mean. A large sample size is needed for high confidence. For a large sample size ($n \ge 30$), the confidence limits for the population mean can be expressed as (Spiegel, 1975):

$$\bar{X} \pm Z_c \frac{\sigma}{\sqrt{n}}$$
 (14)

For a small sample size (n<30), confidence levels can be obtained using the t distribution. The confidence limits are given by:

$$\bar{X} \pm t_c \frac{\sigma}{\sqrt{n}}$$
 (15)

where \overline{X} is the sample mean, σ is the sample standard deviation, and the term $\frac{\sigma}{\sqrt{n}}$ is the standard deviation of the mean. The values of Z_c and t_c correspond to different confidence levels (99.73%, 99.45%, 68.27%, etc.). For example, one can be 68.27% confident that the true mean lies between the interval of $\overline{X}\pm\frac{\sigma}{\sqrt{n}}$ ($Z_c=1$).

The possible sources of systematic error in this study can be generalized as follows:

- (1) Specimen preparation
- (2) Image acquisition
 - Alignment of specimen
 - Lighting
 - Cameras and lenses
- (3) Image processing and analysis
 - Operations applied
 - Setting threshold values
 - Separating touching features
 - Setting spatial calibrations to change spatial measurement units
- (4) Mathematical calculations

Errors encountered in the measurements will be discussed in this Chapter and Chapter 4.

3.4 Braid Angle Determination

3.4.1 Calibration

Test images with known braid angles were created for calibration tests. Since test images are noise free and their complexities are under controlled, they can be used to understand how well computer-based pattern recognition compares to human-based pattern recognition for ideal situations. This is helpful to define the capabilities of performance and the influences on the real situations which are non-ideal. Also with test images systematic errors which may be introduced by the image acquisition, the image processing software and the calculations involved can be detected.

Test images with angles arbitrarily chosen from 30° to 80° were created and digitized. These digitized images are called test raw images. Then the test raw images were transformed into the frequency domain using the FFT operation. The images after applying the FFT operation are called FFT images. Figure 24 shows an example of these images where x1 and x2 are raw angles, x3 and x4 are the corresponding FFT angles.

Another test image which consists of ten non-parallel lines corresponding to ten braid angles (from 42.6° to 51.0°) was created. The average of these ten

braid angles is 46.9°. Figure 25 shows the corresponding FFT image of this test image. It can be seen that the energy spectrum is more widely spread out compared with the one in Figure 24. Image operations were performed on the FFT image to define the influences of the image processing on measurement results and determine the adequacy of the proposed method. Image operations involved will be discussed in section 3.3.2. The FFT image after thinning is shown in Figure 26. Angle measurements were conducted on the final thinned images. Comparison was made between least-squares determinations and manual determinations.

The resolution limits of the measurements are determined by the resolution of the frame grabber (512 x 418 pixels) and the magnifications of the optics. The highest resolution for the angle measurement limited by image digitizing is approximately $0.1^{\circ}(atan\left(\frac{1}{512}\right)\approx0.1^{\circ})$. A spatial resolution of 0.1 mm can be obtained with the magnifications used in this study.

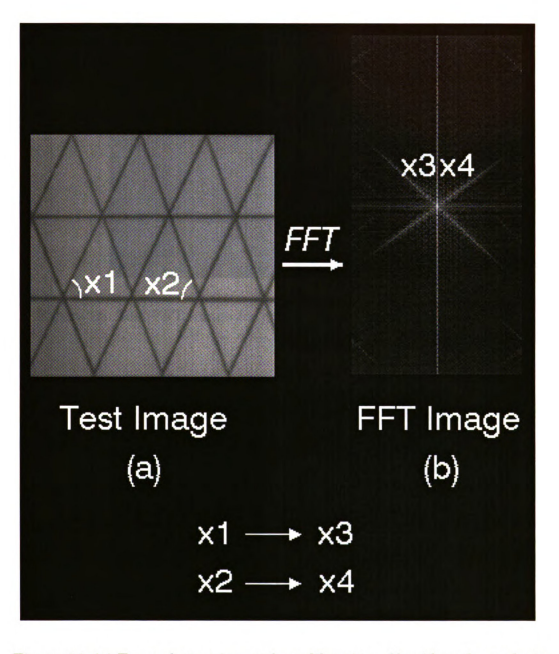


Figure 24. (a) Example test image for calibration of braid angle analysis. (b) The fast Fourier transform of (a).

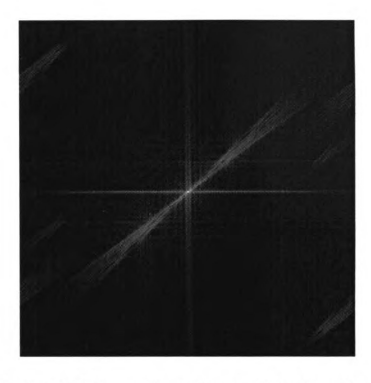


Figure 25. Test FFT image for calibration of braid angle analysis.



Figure 26. Final thinned image.

3.4.2 Sample Image Analysis

Specimen Preparation

The composite components under investigation are triaxially braided glass/urethane parts (crossmembers) provided by Ford Motor Company. Figure 27 shows photographs taken from the real composite part. The method for braid angle analysis considered in the present work is non-destructive. The sample was aligned manually on the baseboard of the photostand (Figure 23). The x and y directions can be adjusted with the aid of the sample edge, rulers, the frame grabber and the image processing program. Images were captured at different locations over the sample flat surface along the entire length of the sample. The domain size of the sample represented by the image can be varied depending on the magnification of the optics. It was found that in general a higher magnification will produce better image quality.



(a)



(b)



(c)

Figure 27. (a) The whole part (~1.5 m long).

- (b) A closer picture of the part surface.
- (c) The cross section of the part (80 x 32 mm²). The bright section is the foam core.

Image Processing

Image processing operations were performed on the raw image in order to get the desired information needed to determine braid angles. The operations applied are as follows:

Raw Image --> Equalization --> FFT --> Lowpass --> Dilation -->

Erosion --> Laplacian --> Threshold --> Thinning --> Final Image

An example raw image after histogram equalization which represents a sample area of about 33 x 24 mm² is shown in Figure 28. Histogram equalization attempts to give the best possible gray level distribution to the image. The contrast of the image and the visibility of the features in the image are improved after applying histogram equalization.

Then the image is transformed into the frequency domain using the FFT operation. Due to the complexities of the structure which include variations of the longitudinal tow direction and the braid tow direction as well as the fiber curvature and the noise from the background, the energy spectrum in the FFT is spread out for the image from the real sample. These introduce difficulties for the determination of fiber directions. Figure 29 shows the FFT image of the image in Figure 28.

Next a lowpass filter is performed on the image to remove the noise. Lowpass filtering will produce a blurred effect on the image. Then two morphology operators: Dilation and Erosion are applied to the image successively. The



Figure 28. Example image from the sample surface after histogram equalization.

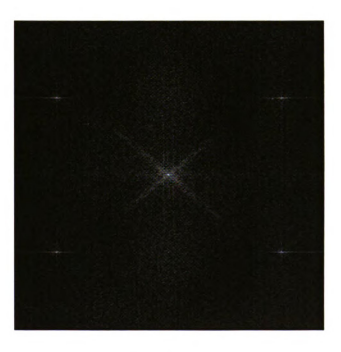


Figure 29. The FFT of the image in Figure 28.

purpose of using Dilation is to connect discontinuous features in the image. As mentioned in section 2.4, as a result of Dilation the object size will be expanded while the following Erosion will reduce the object size. Therefore the overall size of the object can be restored somewhat. The image after applying Dilation and Erosion operations is shown in Figure 30.

The fiber directions are detected using the Laplacian edge detector. The FFT image after Laplacian edge detection is shown in Figure 31. Two main directions which correspond to crossed fiber (braid tow) directions can be recognized from the image.

By thresholding, a gray scale image is converted to a binary image where the features of interest in the image are discriminated from the others. And finally the object in the image are reduced to a single pixel width using the thinning operation.

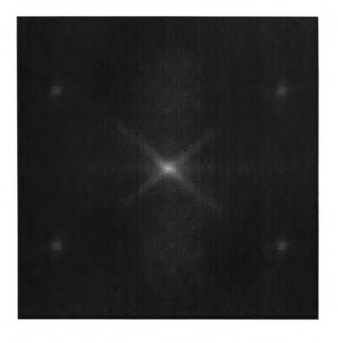


Figure 30. Image produced by applying Dilation and Erosion operations.

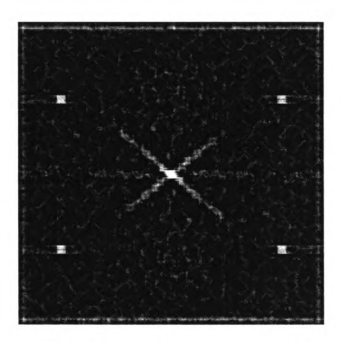


Figure 31. Image in Figure 30 after Laplacian edge detection.

Investigations have been conducted to identify the spectrum distribution of the noise in the FFT image. No definite pattern has been found. This can be done in two ways. One is to apply the FFT to the background. The result shows that the spectrum is randomly distributed over the frequency space. Another way is to remove the frequencies in the defined areas between the main directions, then restore the image using the inverse FFT operation. An image with smooth background is obtained. Figure 32 shows one image after applying the inverse FFT.

When the same processing operations are performed on different images or repeated on one image, the Script Mode of the image processing software can be used to enhance the processing speed. When Script Mode switches on, it records all the operations into a .SCR file. By using Play Script the next time, the selected previously recorded script file will be played back automatically.

Braid Angle Measurement

Images after thinning are used to represent the mean fiber directions. These images are saved as .BIT files in Image-Pro Plus. In a .BIT file an image is represented by a two-dimensional array where each cell in the array has an intensity value that describes the pixel of the image. Least-squares lines were found to approximate the fiber directions in order to calculate braid angles.

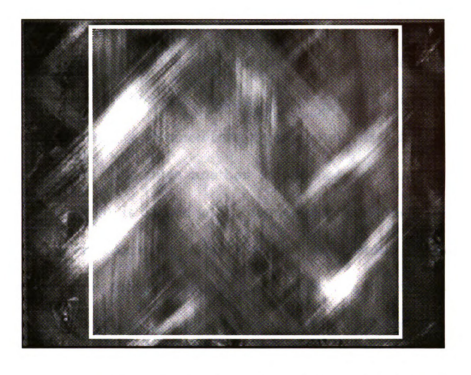


Figure 32. Inverse transformation of the modified FFT in Figure 29.

3.5 Crimp Angle Determination

The general process for the crimp angle measurement includes:

- (1) edge detection;
- (2) identifying the fiber boundary;
- (3) fitting a model function to the fiber boundary;
- (4) using the information from the fitting function to calculate crimp angles.

3.5.1 Calibration

Sinusoidal and polynomial test images with known crimp angle were created and digitized. Without applying any image operation, these images were used to compare results obtained from a polynomial curve fitting with known values. Figure 33 illustrates another polynomial test image. The portion which is set to white is chosen as the representation of the ideal crimp, and the remaining areas are set to black as the background. Image operations were performed on the test image. The operations applied are the same as those applied to the real sample images in order to explore the influence of image processing on the ideal situation which is necessary for investigating the influence of processing operations applied on the quantification of crimp angle when the situation is non-ideal. Discussions will be given concerning the operations involved in the following section. Figure 34 shows the image produced by thresholding. The image in Figure 34 after thinning is shown in Figure 35. This thinned image is used to represent the centerline of the crimp shape in the raw image. A 7th order polynomial was found to approximate the crimp curve.



Figure 33. Polynomial test image for calibration of crimp angle analysis.



Figure 34. Image after thresholding.



Figure 35. Image in Figure 34 after thinning.

3.5.2 Sample Image Analysis

Specimen Preparation

A flat plaque composite sample 48A (one of the three architectures investigated by Ford Motor Company) was used for crimp angle analysis (Jaranson et al., 1993). For each specimen, two cuts were made along the braid tow direction of the sample. The sizes of specimens are different from one to another. Manual polishing was carried out until the desired quality of side surfaces was obtained. Manual alignment of the specimen is required. The mean yarn direction can be determined using the edge of the specimen as a reference and with the aid of the frame grabber and the image processing program.

Image Processing

The crimp images were taken in Dr. Anil Jain's lab. It has been found that properly lighting the sample including the top and bottom illumination has beneficial effects on the image quality. A series of image operations were found to be necessary to process the raw image in order to make it suitable for doing measurements. The operations involved are given below:

Raw Image --> Equalization -->Lowpass -->

Laplacian --> Threshold --> Thinning (Sobel) --> Final Image

Figures 36-42 show a series of image transformations. The actual size of each

image displayed is for a sample size of about 32.2 x 5.5 mm². An example raw image used to determine crimp angle is shown in Figure 36. First histogram equalization is applied to the raw image. It can be seen from Figure 37 that significant improvement of the fiber visibility is obtained after histogram equalization. Then applying a lowpass filter to the image in Figure 37 produces the image in Figure 38. The Laplacian edge detector is used to detect the fiber edges. As a result of applying the Laplacian edge detection filter, the regions with low contrast in the image will be removed and edges will be enhanced. This effect is shown in Figure 39. After thresholding (Figure 40), the Sobel nonlinear edge filter may be used to detect both top and bottom boundaries of the fibers (Figure 41). The result of applying the thinning operation to the image in Figure 40 is illustrated in Figure 42.

This is a general process. Due to the variation of image complexities, for a specific image, repetitions of some operations may be required. When setting the threshold, problems may be encountered associated with separating touching features that have similar gray values. The correct threshold to detect the fibers of interest may also detect other features which are touching the fibers. Therefore in order to separate these features from the fibers, the threshold may be set to a value where the fibers are underdetected. In the case when touching features can not be entirely separated from the fibers by thresholding, then the Sub operation in the image processing software which performs substraction of the specified operand from the image is needed to accomplish this in order to get a nice thinned image. This operation requires



Figure 36. Example raw image for crimp angle determination.



Figure 37. Image in Figure 36 after histogram equalization.



Figure 38. Image in Figure 37 after applying a lowpass filter.

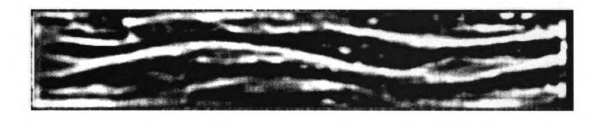


Figure 39. Image in Figure 38 after applying a Laplacian edge filter.



Figure 40. Image in Figure 39 after thresholding.



Figure 41. Image in Figure 40 after applying Sobel filter.



Figure 42. Image in Figure 40 after thinning.

human determination. Otherwise branches and loops may appear at touching points which make the thinned image complicated. Errors may occur during this process. A way to reduce the errors is to observe the closeness of fit between the binary image and the gray level image. This can be done using the Diff operation in the image processing software which gives the absolute value of the difference between the two specified images.

Crimp Angle Measurement

Data from .BIT files were used to calculate the crimp angles. 7th order polynomials were found to approximate the curves. The number of points used to find a polynomial fit is determined by the step size and the horizontal width of the crimp. The portions near the two ends of the curve in the image may be overestimated by the polynomial which does not correctly represent the curve shape. To avoid inaccurate results data from near the ends should not be used for the calculation. For each crimp two crimp angles, one positive and one negative were calculated. The average crimp angle can be obtained by averaging the absolute values of these two angles. This may compensate the initial misalignment of the specimen.

3.6 Fiber Waviness Determination

The determination of fiber waviness is non-destructive. Part of the work has been done for the determination of fiber waviness. It is proposed that similar test images as those used for the crimp angle analysis will be applicable for the calibration work of fiber waviness analysis.

Image operations have been defined to transform the raw image. The techniques involved are quite similar to those used in processing the crimp images. Operations applied are given as follows:

Raw Image --> Equalization --> Vertical Edge -->

Lowpass --> Phase --> Threshold --> Thinning --> Final Image

Vertical Edge is an edge detector which enhances the vertical edges in the image. Other operations involved have been described in the previous sections. Figures 43-46 show an example of such transformations. The curves in the thinned image are used to represent the shapes of the fiber curvature.

For the quantitative determination of fiber waviness, polynomials (6th order) were generated to approximate the fiber curves in Figure 46. It seems that the polynomial approximation or the Fourier series is more suitable than the sinusoidal function for fiber waviness characterization for the real situation. More work needs to be done to quantify the fiber waviness.



Figure 43. Example raw image of fiber waviness after histogram equalization.



Figure 44. Image in Figure 43 after applying a vertical edge filter.



Figure 45. Image in Figure 44 after applying Phase filter and thresholding.



Figure 46. Image in Figure 45 after thinning.

CHAPTER 4

RESULTS AND DISCUSSION

4.1 Braid Angle Determination

4.1.1 Calibration

For the test images with angles arbitrarily chosen from 30° to 80° , ten repetitions of manual angle measurement were performed on each of the test raw images and the corresponding FFT images. The uncertainty is approximately 0.2° for the raw angle measurement and 0.4° for the FFT angle measurement. Results for the test images with the angle range of 30° to 35° are given in Table 1. For each of the ten data sets, a least-squares line was constructed by linear regression analysis of "processed" angle as a function of raw angle. The linear correlation coefficient, r, and the standard error of estimate, S, were calculated. r and S are given by (Spiegel, 1975):

$$r^{2} = \frac{\sum (\theta e s t - \overline{\theta})^{2}}{\sum (\theta - \overline{\theta})^{2}}$$
 (16)

$$S = \sqrt{\frac{\sum (\theta - \theta est)^{2}}{n}}$$
 (17)

where θ is the measured angle, θest is the estimated value of θ using least-squares fit, θ is the mean value of the measured angles, and n is the number of measurements. Results are given in Table 2. The linear correlation coefficient measures how well the least-squares regression line fits the data. From Table 2, it can be seen that good linear correlations are found, since all the correlation coefficients are nearly equal to 1. The standard error of estimate measures the data scatter about the regression curve. An example of fitting a least-squares line to the data points is illustrated in Figure 47. The two broken lines were constructed parallel to the regression line at the vertical distance of S. If the sample points are large enough, then it should be found that 68% of the points would be included between the pair of lines.

For another test image which consists of ten non-parallel lines, measurements were performed on the FFT image after thinning (Figure 26). Two methods, least-squares method and manual measurement were compared. For each case ten measurements were conducted using different threshold values. Results are displayed in Table 3. It can be seen from the table that results from the two methods are in good agreement. The relative errors are comparable. The least-squares method gives a closer result to the known value. It is revealed that the thinned image gives a mean direction in this ideal case. This is expected. The method has been extended to apply to the

real sample analysis. Significant influences on performance have been discussed in section 3.3.2.

Table 1: Calculated Results of Ten Measurements for Each True Angle (Unit: deg)

	,		5		2 2 2 2 2	
קווין	Mean	Mean Value	Standard	Standard Deviation	95% Confider	95% Confidence Limits (±)
Angle	Raw Angle	FFT Angle	Raw Angle	FFT Angle	Raw Angle	FFT Angle
30	30.10	30.03	0.17	0.29	0.13	0.22
30.5	30.53	30.59	0.14	0.35	0.10	0.27
31	31.11	31.26	0.15	0.23	0.11	0.17
31.5	31.48	31.41	0.14	0.39	0.10	0.29
32	32.06	31.96	0.17	0.31	0.13	0.24
32.5	32.52	32.59	0.13	0.34	0.10	0.26
33	32.93	32.85	0.15	0.22	0.11	0.17
33.5	33.50	33.05	0.14	0.31	0.10	0.24
34	34.11	33.86	0.16	0.41	0.12	0.31
34.5	34.55	34.56	0.14	08'0	0.11	0.23
35	34.96	35.00	0.16	98.0	0.12	0.27

Table 2: Calculated Results from Least-Squares Curve Fit

# of Data	Linear Correlation Coefficient		Standard Error of Estimate (deg)	
Set	Raw Angle	FFT Angle	Raw Angle	FFT Angle
1	0.9979	0.9803	0.10	0.32
2	0.9966	0.9704	0.13	0.37
3	0.9973	0.9727	0.12	0.37
4	0.9976	0.9910	0.11	0.23
5	0.9970	0.9753	0.12	0.34
6	0.9948	0.9928	0.16	0.17
7	0.9964	0.9811	0.13	0.31
8	0.9957	0.9920	0.15	0.19
9	0.9956	0.9836	0.15	0.27
10	0.9955	0.9627	0.14	0.41

Table 3: Comparison of the Least-Squares Method with the Manual Measurement for Test Images (Unit: deg)

Method	Measured Mean Angle	Standard Deviation	Known Angle	Percentage Error (%)
Least-Squares	46.66	0.26	46.9	0.5
Manual Measurement	46.40	0.13	46.9	1.1

Percentage error=(Measured angle-Known angle) / Known angle.

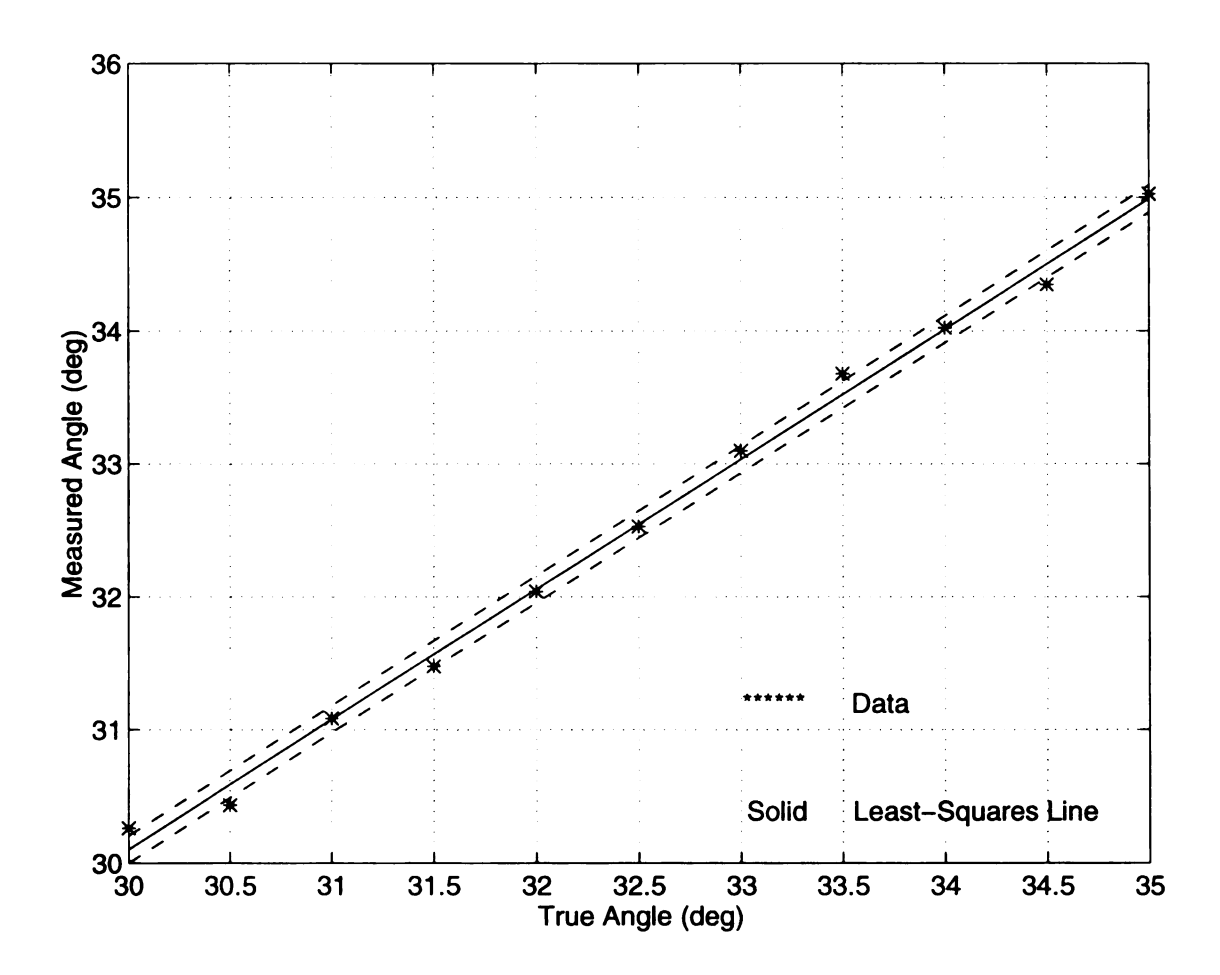


Figure 47. Example of least-squares line fit to data points.

4.1.2 Sample Image Analysis

Images were taken at six different locations along the sample flat surface. Since measurements were conducted over relatively small areas, it is assumed that the waviness of longitudinal fibers is negligible. The FFT only transforms a certain part of the image, within the transformed area of each image about 5-8 braid angles were measured. The right angle corresponds to θ, and the left angle corresponds to the absolute value of -θ. Braid angles, the mean values of right and left angles are given in Table 4. The results suggest that the braid angles vary from location to location. The absolute value of variation is up to 11.14° for the mean values within the measured domain of approximately 1200 x 80 mm². Comparison of the least-squares method with the manual measurement was made. Results are reported in Table 5. The mean of the measurements from the six locations is 45.47° with a standard deviation of 3.38°. This is comparable to the mean of 46.6° and a 3.2° standard deviation obtained from direct manual measuring on the sample surface.

The reproducibility of the braid angle measurement for the real sample has been examined at a single location by investigating the variability introduced by:

- (1) the image transformations with a specified threshold value;
- (2) the image transformations with different threshold values.

Since the shape and the size of the object will change with different threshold values, the result produced by thresholding will directly affect the thinning result. As discussed in section 2.5, thinning is very sensitive to changes

of the object shape. A little change may introduce additional branches, loops or other complicated features. This will make the quantitative analysis difficult and the result may be unreliable. Therefore it is desired to know the influence of the setting of thresholds on the measurement results. Five measurements were conducted for each of the two cases. A mean of 44.13° with a standard deviation of 0.16° for case (1) and a mean of 43.60° with a standard deviation of 0.72° for case (2) are observed. The results suggest that the variation of the braid angle measurement produced by using a fixed threshold value is less than the variation of the braid angle measurement produced by using different threshold values. Compared to the variation of 3.38° observed at different locations in a single sample, the variation level of 0.16°-0.72° is small.

Table 4: Braid Angles at Different Locations (Unit: deg)

Location	Braid	Angle	Mean Value
	Right	Left	Weam value
1	43.28	45.25	44.27
2	46.48	44.09	45.29
3	53.47	48.93	51.20
4	42.79	40.58	41.69
5	47.01	42.59	44.80
6	46.02	45.25	45.64

Table 5: Comparison of Braid Angle Measurements between the Least-Squares Method and the Manual Measurement (Unit: deg)

Method	Mean Braid Angle	Standard Deviation	95% Confidence Limits (±)
Least-Squares	45.47	3.38	1.05
Manual Measurement	45.6	3.2	2.3

4.2 Crimp Angle Determination

4.2.1 Calibration

Angles measured from test images using the polynomial fit method without applying image operations were compared with known angles. Results are displayed in Table 6. It is suggested that the polynomial fit can yield a rather good approximation to the true value (to within approximately 1%).

Ten measurements were performed on another test image (Figure 35). The mean for the measured angle is 12.63° with a standard deviation of 0.20°. Compared with the known angle of 12.95°, a 2.5% percentage error is defined. No significant systematic error which biases the measurement results is found from the image processing.

Table 6: Crimp Angles from Test Images (Unit: deg)

Test Function	Measured Angle	Known Angle	Percentage Error (%)
Sinusoidal Function	45.49	45.00	1.1
Polynomial Function	13.06	12.95	0.8

Different results were found by using different orders of polynomial and different numbers of points to determine the polynomial functions. Investigations were conducted based on the test images. The uncertainty from the choice of polynomial orders (5th, 6th and 7th) is approximately 0.45° . And the uncertainty from changing numbers of fitting points (15-30 points) is approximately 0.13° . It was found that a 7th order polynomial gave a more accurate approximation to the curve shape, since a minimum value of the summation of the square of the errors was obtained for the 7th order polynomial, where the error is the difference between the original value and the corresponding estimated value using polynomial fit.

4.2.2 Sample Image Analysis

Crimp angles were measured on nine specimens. There are typically 2-5 crimps in each specimen. Figure 48 shows an example of polynomial fit to the data points of the fiber boundary. The mean value of the crimp angle $(\overline{\alpha})$,

standard deviation (σ) and the coefficient of variation (the ratio of σ to $\overline{\alpha}$ ($\sigma/\overline{\alpha}$)) were calculated for each specimen. N is the number of crimp angles measured for each specimen. Results are given in Table 7. It can be seen from the table that the crimp angles vary by 6%-36% for different specimens. For a specific specimen the crimp angles change from one location to another along the braid tow direction with a maximum standard deviation of about 4°. The mean crimp angle for the nine specimens is 11.86° with a mean standard deviation of 3.11°. A plot of crimp angles from different specimens is illustrated in Figure 49. The error bars shown in the plot are standard deviations of the mean.

Figure 50 displays the sample crimp angle distribution over a single sample. Sixty-nine crimp angles were measured. The measured mean is 11.75° with a standard deviation of 3.30° . The 95% confidence limits for the measured mean of one sample is $11.75^{\circ} \pm 0.78^{\circ}$ which was calculated using equation (14). This mean crimp angle is comparable to the average crimp angle of 10.6° reported by Jaranson et al. (1993) who found the result by averaging the crimp angles measured from four specimens.

From the above results it is revealed that the variability of crimp angle determinations observed in different specimen (11.86° \pm 3.11°) is almost identical to the variability observed for different locations on a single specimen (11.75° \pm 3.30°).

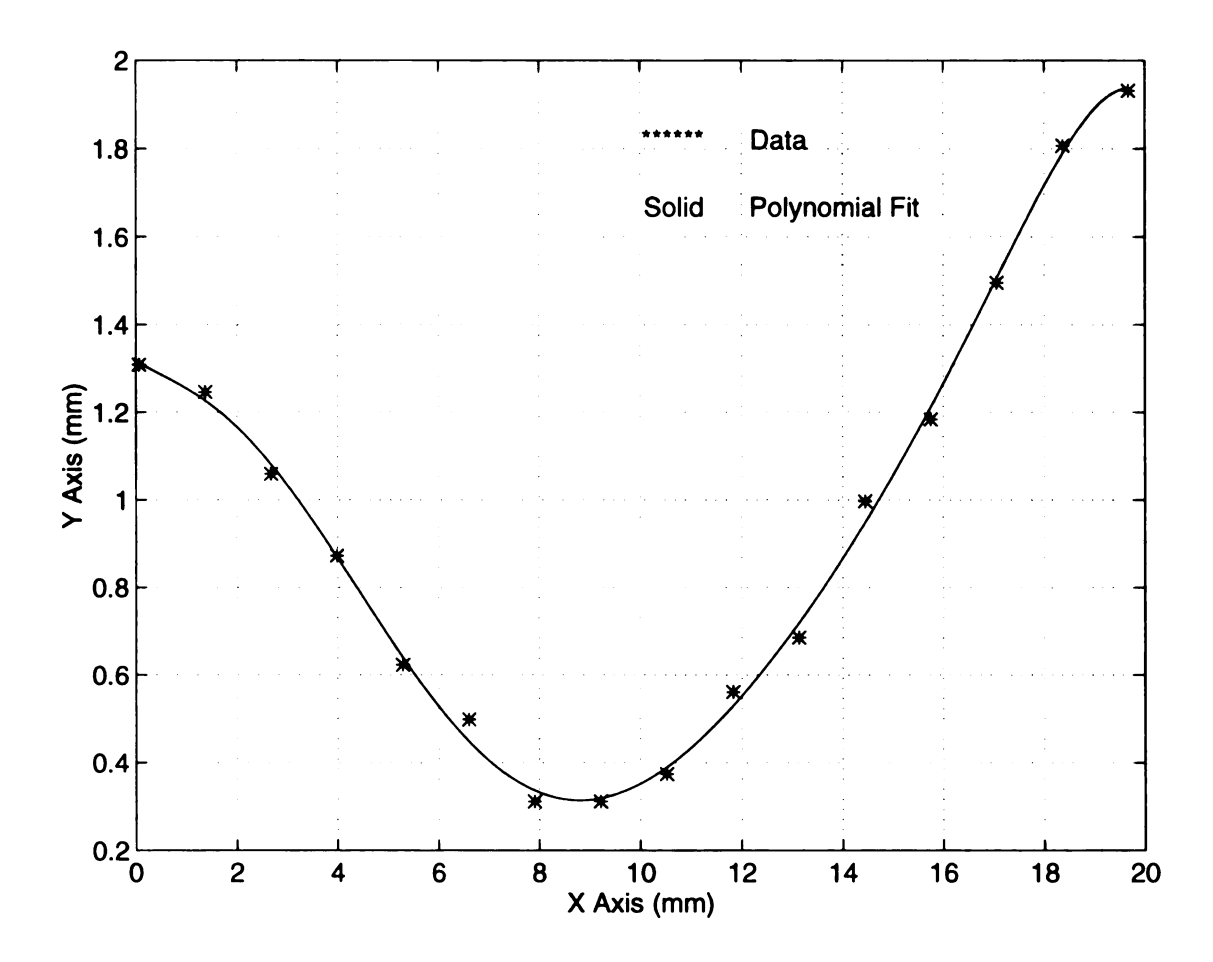


Figure 48. Example of 7th order polynomial function fit to the fiber boundary.

Table 7: Crimp Angles from Nine Specimens (Unit: deg)

Specimen	Mean Crimp Angle $(\overline{\alpha})$	Standard Deviation (σ)	σ/α (%)	N
1	11.48	3.08	27	6
2	10.46	3.72	36	8
3	12.04	3.93	33	8
4	12.52	2.60	21	8
5	11.66	3.23	28	6
6	11.41	3.24	28	9
7	12.80	3.90	30	10
8	13.80	0.87	6	4
9	10.58	3.38	32	10

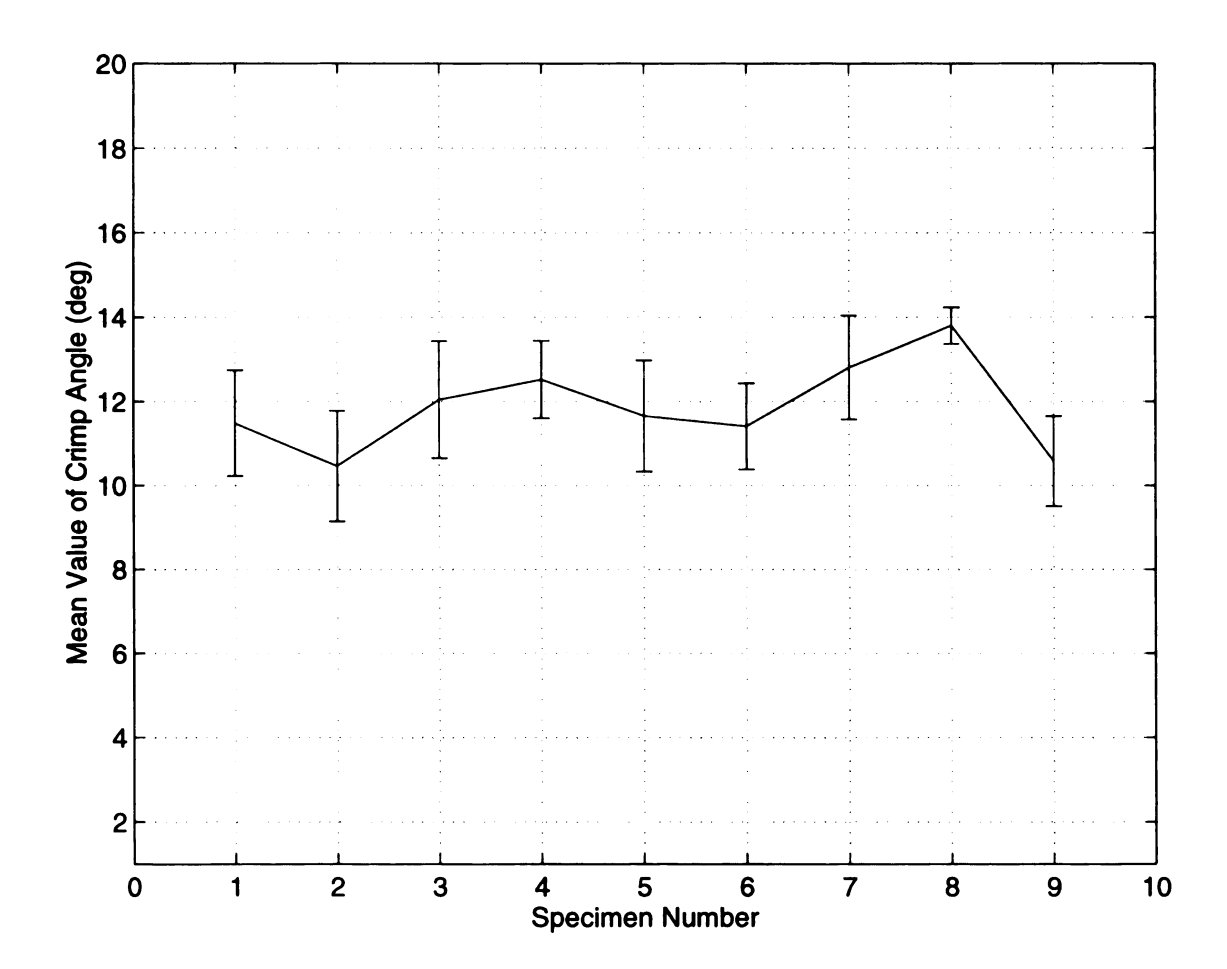


Figure 49. Crimp angles measured on different specimens.

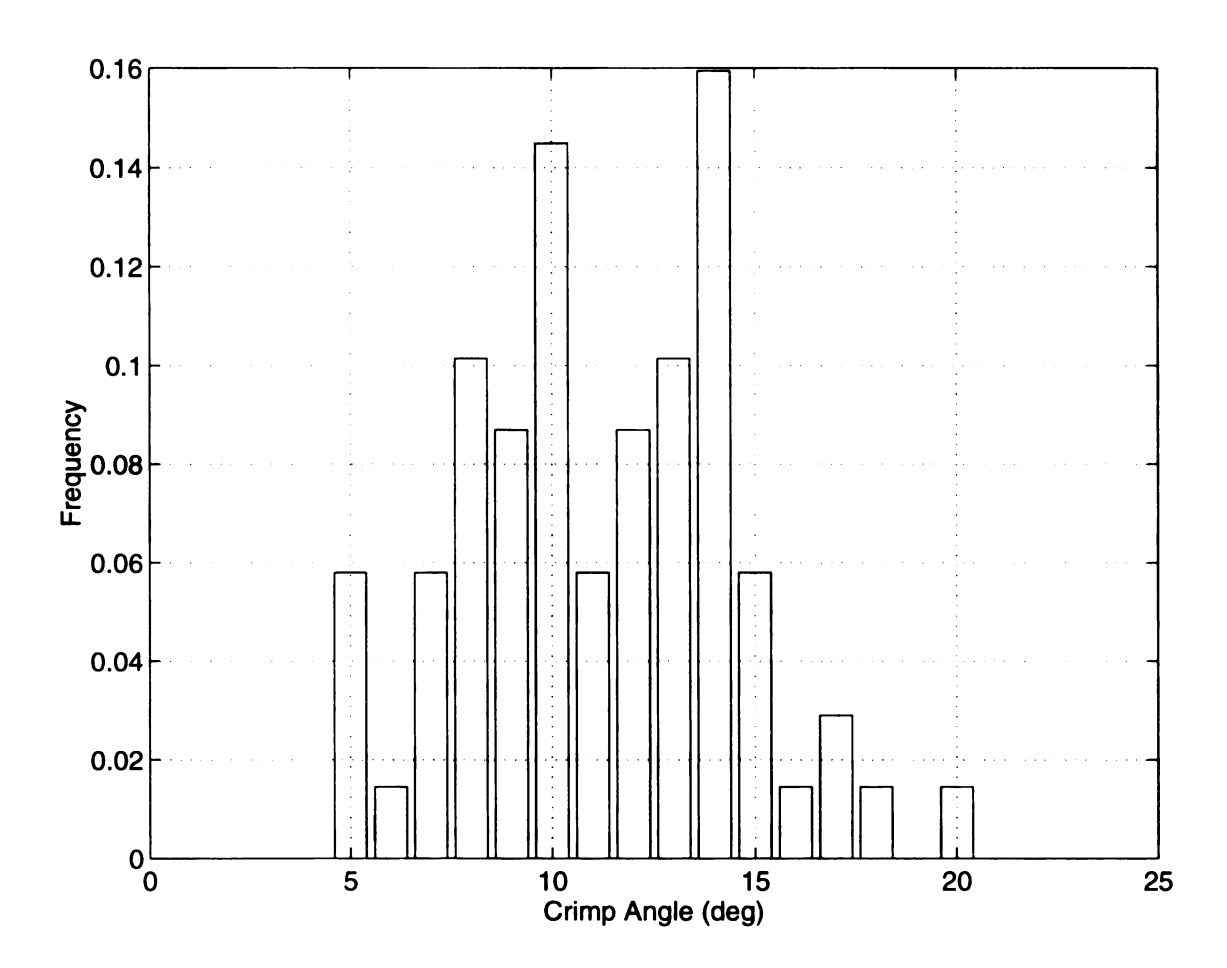


Figure 50. Crimp angle distribution over one sample.

The investigation of the reproducibility of the crimp angle measurement for the real specimen has been conducted by examining the following situations:

- (1) the influence of multiple imaging on one specimen;
- (2) the influence of the setting of thresholds examined at a single location for a given specimen.

Results revealed by Table 8 show that the reproducibility found for one specimen being imaged three times is about 1.0°-1.9° (4%-23% variation). The higher variation of 23% is associated with the lower mean crimp angle (8.32°). It should be possible to reduce this by using higher magnification optics (increasing the resolution of the images).

Table 9 shows the results of the second situation. The standard deviation $(\sigma=0.19^\circ)$ produced by the crimp angle measurement with a fixed threshold value is smaller than the one $(\sigma=0.44^\circ)$ produced by the crimp angle measurement with different threshold values. Five measurements were taken for each situation. It is suggested that using a defined threshold value yields more reproducible results. The variation level of 0.19° - 0.44° is small compared to the variation of 3.30° observed within one sample. As mentioned in section 3.5.2, for the crimp angle determination human involvement is needed to separate touching features. The measurement is insensitive to human interaction judging by the reproducibility results.

Table 8: Reproducibility of the Crimp Angle Measurement Tested by Repeating Imaging on One Specimen (Unit: deg)

Crimp	Mean Crimp Angle $(\overline{\alpha})$	Standard Deviation (σ)	σ/ α (%)
#1	22.48	1.01	4
#2	8.32	1.89	23
#3	10.12	1.16	11

Table 9: Reproducibility of the Crimp Angle Measurement Tested by Repetitions of Measurement on One Image (N=5) (Unit: deg)

Threshold	Mean Crimp Angle $(\overline{\alpha})$	Standard Deviation (σ)	σ/ α (%)
Fixed	12.79	0.19	1.5
Non-Fixed	12.59	0.44	3.5

4.3 Image Analysis Speed

It takes about 5 minutes to capture and transform the image. More time is needed for data processing and quantitative calculations. Presently the total analysis time required is about 14 minutes per image. The time required for the crimp angle analysis is approximately 1-2 minutes longer than for the braid angle analysis due to the human involvement for the determination of crimp angle. The processing speed can be increased with faster equipment (a 120MHz pentium PC and a DT3851 image board). Also the analysis time can be reduced when software subroutines are linked with the existing software to provide curve fitting and quantitative determinations of the morphologies. With such improvement the total time required from imaging the sample to obtaining the quantitative results is expected to be about 8-9 minutes.

CHAPTER 5

CONCLUSIONS AND RECOMMENDATIONS

5.1 Conclusions

The morphological features including braid angle and crimp angle were quantified using computer-aid image processing techniques. Image operations were defined to process the image for the analyses of braid angle, crimp angle and fiber waviness. Calibration results show that braid angles can be measured to within 0.5% and that crimp angles can be measured to within 2.5%. It is suggested that the present methods can produce accurate angle determinations for ideal cases. Based on test images, good correlation is found between computer-based and human-based determinations.

For real sample analyses, the braid angle variation within one sample is found to be about 7% and the crimp angle variation within one sample is found to be about 28%. The results of reproducibility for both braid angle and crimp angle measurements tested by changing threshold values suggest that

using a defined threshold value yields more reproducible results (0.4% for braid angle determinations and 1.5% for crimp angle determinations) than using different threshold values (1.7% for braid angle determinations and 3.5% for crimp angle determinations). Also the reproducibility of the crimp angle measurement tested by multiple imaging on a single specimen is within the range of 4%-23%.

The braid angle determination is non-destructive and based on the fast Fourier transform method. Linear least-squares curve fitting is used to determine the fiber directions. Cutting is presently required to determine the crimp angle. The fiber shape is approximated by a 7th order polynomial function. The quantitative description of fiber waviness has not been entirely accomplished. No significant systematic error was detected for the present methods.

With the Image-Pro Plus version 1.2 for Windows, operator input is eliminated. This is desirable for the automation purpose. Scripting has been used to automate a part of the image transformations. The total time required from imaging the sample to obtaining the final quantitative results is about 14 minutes per image.

The present method is limited to characterizing braid angles at the sample surface regions where the fiber visibility is relatively good. The interior features can not be detected non-destructively with the present approach.

In order to get good statistical representations of the results, good quality images and a relatively large number of measurements are required. Specifically, for braid angle analysis approximately ten images which are taken from each side of the cross member flat surface at different locations are needed.

But in some surface regions the fiber visibility is poor. In this case, the image can not provide any useful information.

5.2 Recommendations for Future Work

Recommendations for the Equipment

Due to the limitations of the present equipment, images being taken using the current video camera (a Javelin Mos Sensor camera with a resolution of 485 x 384 pixels) and lens (a Canon 16-100 mm TV Zoom lens) we can not achieve the desired image resolution and quality level. A CCD B/W video camera (a resolution of 768 x 493 pixels or higher is preferred), a high quality zoom lens and a photostand with top and bottom illumination are required to improve the image quality. The storage space provided by the current PC computer system is far from enough and the time for image analysis needs to be reduced. The situation should be improved with a new pentium PC and the image board. It is suggested that the workstation could provide much greater computational capabilities (Yurgartis, 1994) for digital image analysis. A hard disk tape drive is being used for image backups. The data storage and retrieval are cumbersome and time inefficient. It seems that optical disks might be a better choice for fast data storage, data retrieval and cost-effective.

Recommendations for Quantitative Determinations

Similar strategies as used in the determinations of braid angle and crimp angle including the calibration test and the sample image analysis should be employed to investigate the fiber waviness.

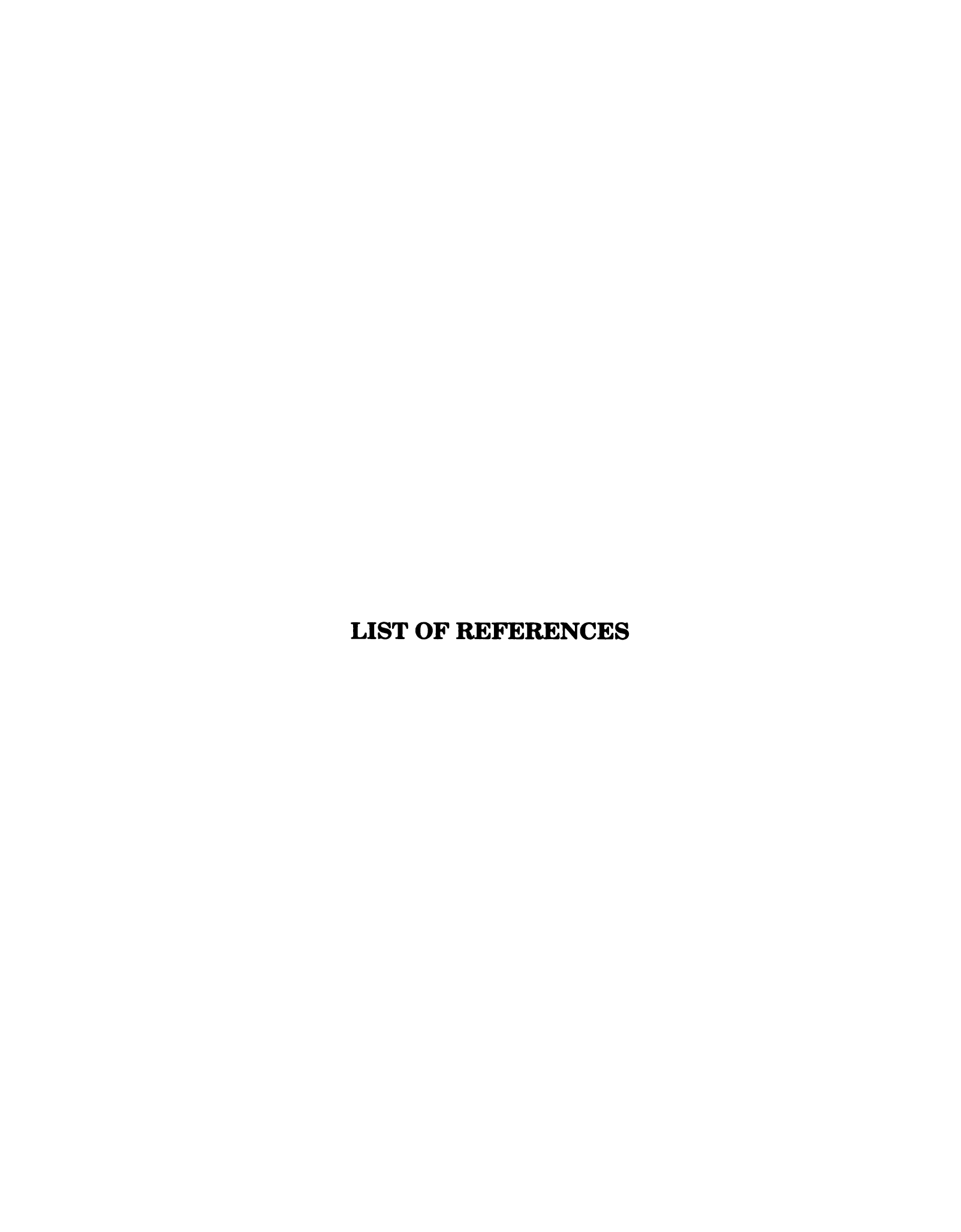
For braid angle and crimp angle determinations, measurements need to be taken to examine the variation of the measurements on different samples. The variability which may be introduced by sampling the same specimen at a specified location by different operators should be investigated.

Presently a flat plaque sample is used for the crimp angle determination due to the poor contrast between fibers and the matrix of the actual structural part, but it is desired to perform analysis on the real crossmember sample in future work. To enhance the contrast it may be useful to include some opaque "tracer" fibers in the braiding process. Also some modifications of the imaging method may be helpful such as using color filters or polarizing filters.

Preliminary work on the braid angle determination has been done using x-ray photographs which were provided by Ford research engineers. The photographs were imaged, then these images were transformed into the frequency domain. One problem associated with using the photographs is the quality of the image. More work needs to be done to investigate the feasibility of using photographs as the source to quantify braid angles. Other techniques could be investigated such as an ultrasonic nondestructive evaluation method or IR imaging radiometry technique to explore the possibilities for determining the interior braid angles and crimp angles non-destructively.

Automating the entire analysis process is the long term goal of this study.

A part of the future work will be writing subroutines and linking with the existing software to provide automated morphological feature determinations.



LIST OF REFERENCES

Blake, R. A., Jr (1987), "Image Processing of Composite Materials Using Ultrasonic Nondestructive Evaluation Data", Non-Destructive Testing of Fibre-Reinforced Plastics Composites, Vol. 2, ed. J. Summerscales, Elsevier Applied Science, New York, pp. 161-200.

Castleman, K. R. (1979), "Digital Image Processing", Prentice-Hall, Inc., New Jersey.

Cole, G. S. (1991), "Practical Examples of Useful Algorithms in Computer-Aided Microscopy", Micon 90: Advances in Video Technology for Microstructural Control, ed. George F. Vander Voort, ASTM, Philadelphia, pp. 5-28.

Gonzalez, R. C. and Wintz P. (1977), "Digital Image Processing", Addison-Wesley Publishing Company, Massachusetts.

Gowayed, Y. A. and Russ, J. C. (1991), "Geometric Characterization of Textile Composite Preforms Using Image Analysis Techniques", Journal of Computer-Assisted Microscopy, Vol. 3, No. 4, pp. 189-199.

Hussain, Z. (1991), "Digital Image Processing: Practical Applications of Parallel Processing Techniques", Ellis Horwood, England.

Jaranson, J., Pastore, C., Singletary J., Field, S., Kharod, A. M., Kniveton, T. and Rushing, H. (1993), "Elastic Properties of Triaxially Braided Glass/Urethane Composites", Proceedings of the 9th Annual ASM/ESD Advanced Composites Conference, pp. 359-377.

Jortner, J. (1989), "Effects of Crimp Angle on the Tensile Strength of a Carbon-Carbon Laminate", Symposium on High Temperature Composites-Proceedings of the American Society for Composites, Technomic Publishing Co., Lancaster, PA, USA, pp. 243-251.

Masters, J. E., Foye, R. L., Pastore, C. M. and Gowayed, Y. A. (1993), "Mechanical Properties of Triaxially Braided Composites: Experimental and Analytical Results", Journal of Composites Technology & Research, Vol. 15, No. 2, Summer, pp. 112-122.

Rai, H. G., Rogers, C. W. and Crane, D. A. (1992), "Mechanics of Curved Fiber Composites", Journal of Reinforced Plastics and Composites, Vol. 11, pp. 552-566.

Russ, J. C. (1990), "Computer-Assisted Microscopy: The Measurement and Analysis of Images", Plemum Press, New York.

Russ, J. C. (1995), "The Image Processing Hand Book", Second Edition, CRC Press, Florida.

Spiegel, M. R. (1975), "Probability and Statistics", McGraw-Hill, New York.

Taylor, J. R. (1982), "An Introduction to Error Analysis", University Science Books, California.

Xu, B., Pourdeyhimi, B., and Sobus, J. (1992), "Characterizing Fiber Crimp by Image Analysis: Definitions, Algorithms, and Techniques", Textile Research Journal 62 (2), pp. 73-80.

Yurgartis, S. W. (1987), "Measurement of Small Angle Fiber Misalignments in Continuous Fiber Composites", Composite Science and Technology, 30, pp.279-293.

Yurgartis, S. W. (1994), "Techniques for the Quantification of Composite Mesostructure", Mesostructures & Mesomechanics in Fibre Composites, Proceedings of 1st International Specialist Meeting, ed. M. R. Piggott, pp. 32-55.

Yurgartis, S. W., Morey, K. and Jortner, J. (1993), "Measurement of Yarn Shape and Nesting in Plain-Weave Composites", Composite Science and Technology 46, pp. 39-50.

